Lin, Z., Liu, X. and Lotfian, S. (2021) Impacts of water depth increase on offshore floating wind turbine dynamics. Ocean Engineering, 224, 108697.
(doi: 10.1016/j.oceaneng.2021.108697)

There may be differences between this version and the published version. You are advised to consult the publisher's version if you wish to cite from it.

http://eprints.gla.ac.uk/238780/

Deposited on: 16 April 2021

Enlighten – Research publications by members of the University of Glasgow
http://eprints.gla.ac.uk

Impacts of water depth increase on offshore floating wind turbine dynamics

Zi Lin[1], Xiaolei Liu[2*], Saeid Lotfian[3]

[1]Department of Mechanical & Construction Engineering, Northumbria University, Newcastle upon Tyne NE1 8ST, UK

[2]James Watt School of Engineering, University of Glasgow, Glasgow G12 8QQ, UK

[3]Department of Naval Architecture, Ocean and Marine Engineering, University of Strathclyde, Glasgow G4 0LZ

[*]Corresponding author, E-mail: Xiaolei.Liu@glasgow.ac.uk

Abstract

This paper aims at investigating the effect of water depth increase on the global performance of a floating offshore wind turbine, with a special focus on the environmental loading effects and turbine operating status. An integrated aero-hydro-servo-elastic (AHSE) analysis was simulated in the time domain. The model was first validated against published results in terms of mooring system restoring force and platform natural frequencies. The considered water depth is between 200 and 300 m, which is the deep-water range used in the current floating offshore wind turbine (FOWT) industry. In this study, both normal operating and failure conditions were considered. Key conclusions from case studies indicated that, based on the current water depth range, platform heave motion with slack mooring configurations and mooring line top tension are more sensitive to water depth. Water depth increase influences the tower base bending force when the turbine has a high-speed shaft brake due to grid loss, but the effects are restricted to the high-frequency response range (>2 Hz) and less obvious than the influences on mooring lines.

Keywords

FOWT; failure condition; water depths effects; slack mooring; taut mooring

Nomenclature

Abbreviations

AHSE	Aero-hydro-servo-elastic
BEM	Blade Element Momentum
BVP	Boundary Value Problem
DEL	Damage Equivalent Load
DFT	Discrete Fourie Transform
DOF	Degree of Freedom
FOWT	Floating Offshore Wind Turbine
FPSO	Floating Production Storage and Offloading

HSS	High-speed Shaft
IEC	International Electrotechnical Commission
JONSWAP	Joint North Sea Wave Project
LC	Load Case
NREL	National Renewable Energy Laboratory
NTM	Normal Turbulence Model
PSD	Power Spectral Density
QTF	Quadratic Transfer Function
SWL	Still Water Level

Symbols

ω	Circular Frequency
φ	Local inflow angle
$b(\omega)$	Radiation Damping
ρ	Water Density
A_k and A_l	Complex wave amplitude
$F_{mooring}$	Mooring force
F_{seabed}	Forces due to seabed and mooring line interaction
F_v	Viscous force
F_{wave}	Wave force
F_{wind}	Wind force
L_{ji}^{RF}	Load range about a fixed load-mean value
M^a	Added mass
U_0	Current velocities
$U_{sub\_surface}$	Sub-surface velocity
V_{total}	Total wind velocity

n_j^{STeq}	Total equivalent fatigue counts for the j[th] time series
z_d	Vertical position of the water particle
Φ_w	Incident wave potential
γ^r	Peak enhancement factor
ζ_a	Wave amplitude
c_b	Damping coefficients
h,d	Water depth
k	Wavenumber
K	Stiffness matrix
k_b	Stiffness coefficients
M	Mass
N	Number of waves
n,l,m,j	Number index
r	Local radius
R	Retardation function
t	Time
ε	Random phase

1. Introduction

The UK government's new vision of power every home through offshore wind by 2030 necessitates a substantial advancement of innovative offshore wind technologies (Durakovic, 2020). This goal can be achieved by significant growth in the offshore wind sector, with larger turbines to be developed in deeper water depths. In addition, the EU offshore wind industry has boosted since last few years, reaching to 3,627 MW new capacity installations in 2019, with a trend of continues expansion of wind farm size and moving to deeper water depths (Walsh, 2020). Worldwide, the majority of the seawater depth, for example, over two-thirds of US coastal areas and European locations, suitable for wind turbine installations is floating solutions (Simos et al., 2018), which has triggered the offshore wind industry gradually moving to deeper water depths.

Offshore wind turbines are sited on fixed or floating platforms. Fixed foundations, such as gravity and monopile types, are restricted to a maximum water depth of 15 and 30 m, respectively (Nagababu et al., 2017). However, from an economic prospect of view, a fixed base starts to lose its advantage for water depths larger than 60 m (Goupee et al., 2014). Water depth is one of the key factors in identifying foundation technology (Nagababu et al., 2017). More specifically, for floating structures with mooring lines, water depth is well known to be a critical parameter in system design, as illustrated by Luo and Baudic (Luo and Baudic, 2003): mooring line length, material and configuration are required to satisfy strict criteria. Currently, fewer studies have focused on mooring system design & analysis with increased water depths. It is widely agreed that a large number of parameters related to the design & analysis of floating offshore wind turbines (FOWTs) need to consider the variety of water depths. The corresponding trend and analysis methods have been learnt from the offshore oil & gas industry. More specifically, when water depth increases, the length and type of mooring lines are adjusted to provide the most effective stiffness for station-keeping purpose. With the growth of water depths, the dynamics of mooring lines are becoming more vital than relative shallower water depth scenarios, which has an emphasis on relying on the coupled system analysis rather than an un-coupled analysis. Generally speaking, water depth effects for moored structures could be divided into two categories:

- One stern from the wave forces in the wave-structure interaction problems, showing a water depth-dependent character, especially in shallow water range.
- The other comes from the interaction between the floating support structure, showing a different level of coupling effects and the dynamic motion responses of the whole system. For most of the moored offshore structures, these coupling effects are stronger in deeper water depth.

For the first category, a widely accepted numerical simulation framework is under the potential flow theory and focuses on the floating body only. Moreover, the adopted assumption is the evaluation of wave forces are not strongly coupled with mooring line dynamics, and therefore the system global performance is often calculated by an un-coupled way in the frequency domain. Both water wave theories and wave forces are depth-dependent. A number of relevant studies have been investigated intensively and are of great significance for the design & optimization of offshore floating structures. The amplitude of second-order forces are much smaller than that of the first-order counterparts, but the difference and sum-frequency components of second-order forces are essential as they are of the potential for trigger slowly varying responses or high-frequency oscillations, respectively (Roald et al., 2013). More specifically, ship-shaped floating support structures like floating production storage and offloading (FPSOs) are sensitive to surge excitation due to their low damping in surge direction (Bayati et al., 2015). In terms of FOWTs, the types of support structures have seen a large variety, but the water-plane area has a much smaller dimension compared to FPSOs. Nonetheless, nonlinear wave forces remain significant for the support structure design & optimization of

FOWTs. To this end, Roald *et al.* (Roald et al., 2013) compared the level of significance of different loading sources applied on FOWTs, showing that, for a Spar-type FOWT, the second-order forces are likely to excite eigenfrequencies, although the level of magnitude of the mean drift force is much smaller than that of mean turbine thrust force. In another example, Duarte *et al.* (Duarte et al., 2014) analysed the effects of second-order wave forces on a Spar-type 5 MW offshore wind turbine. It is concluded that using Newman's approximation (Newman, 1974) underestimated pitch response of the FOWT, regardless of normal of extreme sea states.

Another consideration has focused on the subsequent effect from the interaction between the mooring lines and the floating body, which is also considered as the coupling effects. For shallower water depth, tradition mooring materials include heavy mooring chains and usually formed in a spread mooring configuration. The weight of mooring chains, compared to the floating body, results in a weak coupling effect between the floating body and the mooring lines. Therefore, motion responses and global performance are often carried out in a non-coupled mothed. With the upsurge of water depths, the coupling effects between floating bodies and mooring lines are becoming increasingly central. Moreover, the components of low-frequency responses out surge the other motion components in deep water depths. For example, Bayati et al. (2015) analysed the effects of water depths for a semisubmersible type FOWT. The water depth ranges from 30 to 200 m. It is claimed that water depths have a greater influence on heave motion than surge motion when water depth decreases from 200m to 30m. Chen et al. (2019)analysed the motion response of the wind turbine support platform considering water depth effects. It is claimed that the effects of water depth mainly happened in shallower water depths. From a structural safety point of view, water depths effects need to be considered during the design process and the motion analysis of floating wind turbines. It needs to be pointed out that Chen et al. (2019)'s investigations were based on an un-coupled analysis, without considering the coupling effects between wind turbine aero-hydro-servo-elastic (AHSE) and mooring line dynamic responses. Wen et al.(2018) designed a short new spar floating vertical axis offshore wind turbine, aiming at operating in a moderate water depth range, based on the feasibility of fully coupled time-domain numerical simulation. It is demonstrated that the new spar outperformance the original design in terms of platform horizontal motion responses and tower side-side bending moments. (Le et al. (2019) proposed a new submerged offshore wind turbine aiming at operating in intermediate water depths between 20 and 200 m. Feasibility studies were put forward concerning different environmental conditions, tether length, tether pretension and tether failure scenarios. It is claimed that tether length contributes to the surge, heave pitch and yaw motion responses.

As a result of more stable wind resources in offshore locations, this paper contributes to investigating the effects of water depth increases for deepwater FOWTs using an integrated AHSE analysis and considers the nonlinear hydrodynamics of the support structures. To sum up, this paper aims at bridging the following knowledge gaps:

- Currently, wind turbines operating in water depth for larger than 50 m are being developed (Nagababu et al., 2017). Worldwide, the majority of offshore areas, such as the west coast of the US and Japan are of the range of deep water and suitable for FOWTs. Moreover, many countries have set up the carbon footprint reduction goals, with the offshore floating wind industry to be contributed significantly to achieving these aims. However, the effects of an increased water depth for FOWTs have not been precisely studied in previous studies. Hence, this paper aims to investigate the effects of water depth increases on the global motion responses and mooring dynamics, offering recommendations for wind turbine designer on developing a new wind farm in deep water areas.
- The progress of mooring materials for station keeping purpose has seen a significant improvement since the past few decades. In the oil & gas sector, the definition of deepwater refers to the level of thousands of meters, which is significantly different from the current deep-water range for FOWTs (~ 300 m). As the length and the cost of mooring lines are proportional to water depths, the suitability of mooring configurations in terms of deep water for oil & gas platforms needs to be re-accessed when it comes to FOWTs. Besides, even though the theory, design and method of analysis for FOWTs originated from offshore oil & gas platforms, the present of the wind turbine and the aerodynamics from wind-structure interactions play a significant role in determining the global performance of the FOWT platform. Nowadays, one of the major difficulties in preventing the offshore wind industry moving to deeper water is the high costs. Tradition catenary mooring configurations with chains will result in a surge in expenses, while a taut mooring configuration could potentially reduce the charges in larger water depth. Therefore, both spread and taut mooring configurations are considered in this study, together with water depth effects.
- Failure analysis is extremely significant for wind turbine safe operations, which will support in preventing malfunctions and further reduce the costs in daily maintenance. Previous studies have focused on the failure conditions with one mooring line broken (Bae et al., 2017), blade pitch actuator failure (Jiang et al., 2014) and blade structure failure (Ozturk et al., 2018). It should be noted that these failure conditions are focused on one water depth only, although water depth is considered as a non-ignorable design factor. On this account, the case studies carried out in this study include both normal operating and wind turbine failure conditions under a variety of water depths.

2. Methodology

This paper applied an integrated AHSE numerical modelling approach for exploring the global performance of FOWT dynamics under different water depths. The numerical outputs generated from the AHSE model are subsequently feeding to the post-processing analysis for carrying out statistical analysis and fatigue analysis. A sketch of the methods applied in this paper is described in **Fig. 1**. The baseline wind turbine was designed to operate in the water depth of 200 m and the other two water depths were developed based on the parameters in this water depth (see section 4.2). Both normal operating and turbine failure conditions were considered in this paper. All the case studies were carried out in a wind, wave and current loading environment, with different average wind speeds considering both below-rated and above-rated scenarios, respectively.

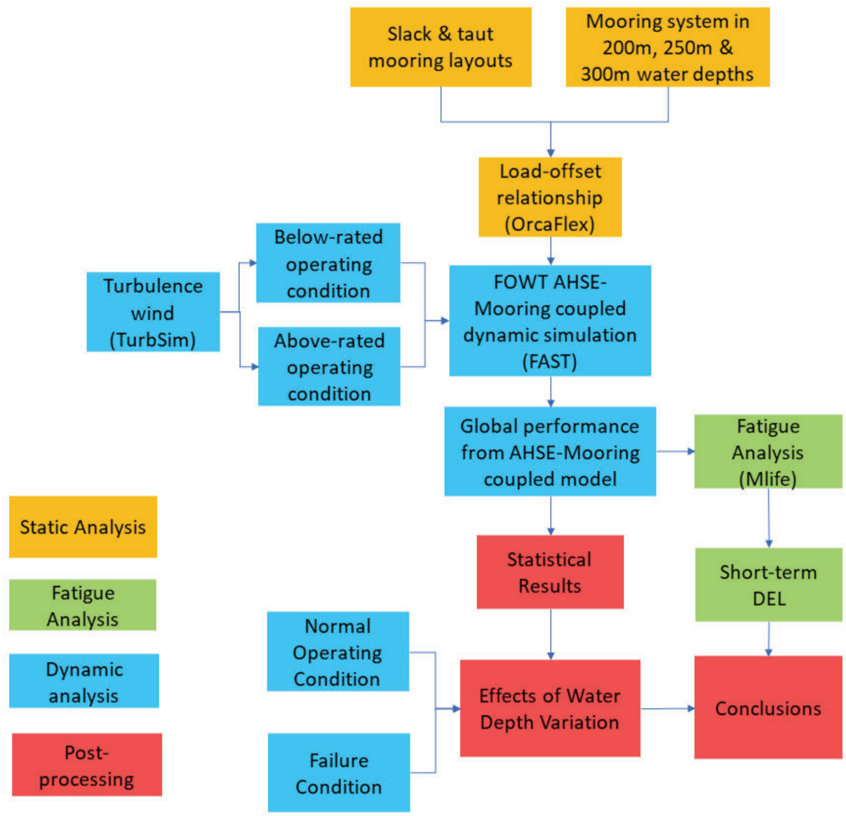

Figure 1 Processes of designed numerical simulations and analysis methods

2.1. Numerical modelling of FOWT

2.1.1. Hydrodynamics

For regular waves, the Airy wave theory is applied to evaluate the wave propagation, determined by a sinusoidal wave elevation(Aggarwal et al., 2017):

$$\zeta = \zeta_a \cos(kx - \omega t) \tag{1}$$

where ζ_a is the wave amplitude, k is the wavenumber, ω is the wave frequency, and t is the time. The corresponding incident wave potential Φ_w in finite water depth can be written as (Journée and Massie, 2001):

$$\Phi_w = \frac{\zeta_a g}{\omega} \cdot \frac{\cosh k(h+z_d)}{\cosh kh} \cdot \sin(kx - \omega t) \tag{2}$$

where h is the water depth and z_d is the vertical position of the water particle.

For irregular waves, a superposition theory, based on the linear wave theory, is applied to calculate the long-crested random wave propagation. The approximation to first-order incident wave is sufficient to investigate the second-order wave force effects, including sum and difference frequency components. For long-crested seas, the incident wave elevation for random waves can be determined by the summation of a number of regular wave components (Journée and Massie, 2001):

$$\zeta(t) = \sum_{n=1}^{N} \zeta_{a_n} cos(k_n x - \omega_n t + \varepsilon_n) \tag{3}$$

where n describes the number index, N is the number of wave compounds, and ε is the random phase.

For wave-structure interaction problems, the added mass, radiation damping and wave exciting forces were calculated in the frequency domain, before running a time-domain mooring system analysis. In view of the submerged structure dimension, full Quadratic Transfer Function (QTF) was considered in terms of evaluating the wave structure interaction problems, which was realised through establishing the boundary value problem (BVP) up to the second-order perturbation expansion. More specifically, the second-order summation-frequency and difference-frequency are calculated by using the direct method through WAMIT (“WAMIT® WAMIT, Inc.”).

2.1.2. Aerodynamics

The numerical simulation of wind-structural interaction problems has been divided into two steps. The first step includes generating the time series of undisturbed inflow turbulence wind. The input parameters for the turbulence wind generation follow the design standards recommended by IEC-61400-3 (IEC, 2019). More specifically, Kaimal spectrum model together with a turbulence intensity of the inflow wind was applied in the power spectral density for the turbulence wind. To account for wind shear effects, mean u-component wind speed across the rotor disk is calculated by the power-law wind profile:

$$\overline{u}(z) = \overline{u}_{hub} \left(\frac{z}{H_{hub}}\right)^{PLExp} \tag{4}$$

where z denotes the height above ground level, H_{hub} is hub height, $\overline{u}_{hub}$ is the wind speed at hub height, and the value of *PLExop* is 0.14 for Normal Turbulence Model (NTM), following the recommendations by the International Electrotechnical Commission (IEC).

The second step includes evaluating the wind loading on wind turbine blades using the blade element momentum (BEM) theory. The total forces and moments acting on the blade span can be evaluated by an integration of the discrete elements (Deo et al., 2018).

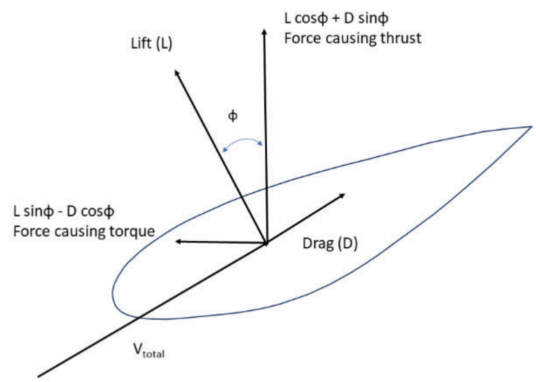

Figure 2 Local element forces

Fig. 2 shows a sketch of the definition of local element sectional forces and their components. The forces are divided into two parts. One is parallel to the rotor plane, which is the torque of the rotor, and the other one is perpendicular to the rotor plane, which is the thrust force.

2.1.3. Structure and mooring models

Dynamic motion responses of the FOWT were evaluated in the time domain. A combined mode shape representation and multi-body analysis were applied for the FOWT dynamic responses. Before running time-domain FOWT dynamic analysis under sea environments, the mode shapes for the tower and the blade were calculated using the BModes (Bir, 2007)computational tool built by National Renewable Energy Laboratory (NREL). Based on Cummins's impulse response function theory (Cummins, 1962), the frequency-dependent wave exciting force, added mass, and radiation damping was converted into time-domain exciting force, infinite added mass matrix and retardation function, respectively. The floating body equation of motion can be written as:

$$[M + M^a(\infty)]\ddot{x} + Kx + \int_{-\infty}^{t} R(t-\tau)\dot{x}(t)\,d\tau = F_{wave} + F_{wind} + F_{mooring} + F_v \quad (5)$$

where M and M^a are mass and added mass; K is the stiffness matrix; F_{wave}, F_{wind} and $F_{mooring}$ are the wave, wind and mooring forces, respectively; F_v is viscous force. The retardation function (R) can be evaluated by:

$$R(t) = \frac{2}{\pi}\int_0^{\infty} b(\omega)\,cos(\omega t)\,d\omega \quad (6)$$

where $b(\omega)$ is radiation damping. F_{wave} includes first and second-order wave exciting forces, which were evaluated in the frequency domain without mooring lines and transferred into the time domain using Discrete Fourie Transform (DFT). As a consequence of the water depth effects carried out in the time domain and focused on the global performance of the FOWT, the wave forces for different water depth assumed unchanged. The first and second components of wave exciting forces can be evaluated as (Roald et al., 2013):

First-order forces ($F_{ex_i}^{(1)}$, i=1, 2, …, 6):

$$F_{ex_i}^{(1)} = Re\left(\sum\nolimits_{m=1}^{N} A_m F_i(\omega_k)^{e^{j\omega_k t}}\right) \tag{7}$$

Second-order forces:

$$F_{ex_i}^{(2)} = Re\left(\sum_{m=1}^{N}\sum_{l=1}^{N}[A_m A_l F_i^{+} e^{j(\omega^{+})t} + A_m A_l^{*} F_i^{-} e^{j(\omega^{-})t}]\right) \tag{8}$$

where $\omega^{+} = \omega_m + \omega_l$ and $\omega^{-} = \omega_m - \omega_l$; k and l are member index; A_m and A_l are complex wave amplitude; The asterisk (*) indicated the complex conjugate. Apart from wave loadings, water particle movements due to sea currents effects were also taken into consideration in the present study. The modelling approach of current-structure interaction follows the standard method as refined in IEC 61400-3 (IEC, 2019):

$$U_{sub\_surface} = U_0 \left(\frac{z+d}{d}\right)^{\frac{1}{7}} \tag{9}$$

where d is the water depth, z is the vertical coornidate, and U_0 denotes the current velocity.

As the above wave-structure interaction modelling is based on potential flow theory, the augmented viscous damping from potential flow loads is realised through the viscous drag term from Morison's equation (Morison et al., 1950).

By using the coupled time-domain simulation method, the effect of mooring line damping and the interaction between the mooring line and the floating body are accounted for automatically. A lumped-mass model (Hall and Goupee, 2015) is used for the dynamic response of the mooring line and realised through the MoorDyn Module of FAST (Hall, 2017). Numerical modelling of mooring line considered hydrodynamic loadings (Morison et al., 1950) and a linear stiffness representation (Bach-Gansmo et al., 2020). For slack mooring chains with a certain component on the seabed, it is important to model the dynamic interactions between the horizontal mooring line and the seabed. To this end, a linear spring-damper model was applied to model the vertical force from the seabed. For a node in the lumped-mass model, the force related to mooring line-seabed interaction (F_{seabed}) can be written as (Hall and Goupee, 2015):

$$F_{seabed} = (z_{bottom} - z)k_b - zc_b \tag{10}$$

where k_b and c_b are the stiffness and the damping coefficients, respectively. The equation is only active when z is lesser than or equals to z_{bottom}.

2.1.4. Fatigue analysis

For a better comparison and understanding of the water depths effects for FOWTs, one of the post-processing procedures cover the fatigue analysis of the FOWT mooring line dynamic time histories. More specifically, the short-term damage equivalent load (DEL) was applied to analyse each output time series. The DEL about a fixed mean is based on an open-source simulation code Mlife (Hayman, 2012), and can be evaluated as follows:

$$DEL_j^{STF} = \left(\frac{\Sigma_i\left(n_{ji}\left(L_{ji}^{RF}\right)^m\right)}{n_j^{STeq}}\right)^{\frac{1}{m}} \tag{11}$$

where j denotes the time series number, n_j^{STeq} is the total equivalent fatigue counts for the j[th] time series, and L_{ji}^{RF} is the corrected load range about a fixed mean cor cycle *i*, time series *j*. The damage accumulates follow a linear assumption, as recommended by the Miner's Rule (Miner, 1945).

3. Model Descriptions and Validations

3.1. Description of the target wind turbine

The present study selected a baseline offshore wind turbine designed by NREL - the 5MW OC-4 DeepWind FOWT (Robertson et al., 2014). The wind turbine is supported by a Semisubmersible-type platform, moored by three symmetrically oriented catenary chains, operating in a water depth of 200 m. Detailed characteristics of the target wind turbine are shown in Robertson et al.(2014), while the layout of the wind turbine mooring system and the definition of environmental conditions are shown in **Fig. 3 and Fig. 4**. For mooring arrangements in **Fig. 4**, the horizontal and the vertical distances between fairlead and anchor indicate the FOWT in 200m water depth. For the remaining water depth (250m and 300m) the arrangement follows the same configuration as **Fig. 4** (three symmetrically oriented lines), but with different horizontal and vertical distances. The detailed anchor positions are described in **Table 3**.

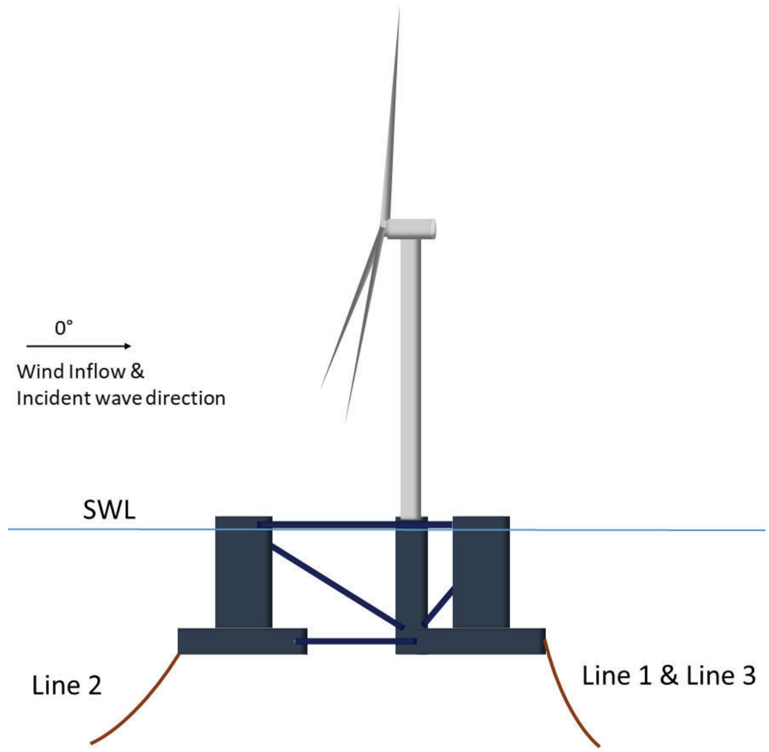

Figure 3 Sketch of the FOWT along with mooring system

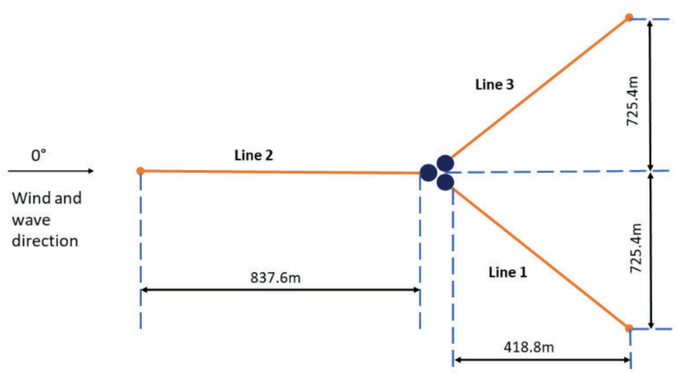

Figure 4 Sketch of the mooring system arrangement (200 m water depth)

The top of the tower has an elevation of 87.6 m above the still water level (SWL), which is consistent with the NREL 5 MW baseline wind turbine for a land-based design. There is a 10 m length elevation between the tower base and the SWL. The main column of the supporting platform has a diameter of 6.5 m, which matches the tower base diameter. The submerged section of the semisubmersible consists of the main column, connecting to the tower and three offset columns with 12 m diameters. The depths between platform base and SWL is 20 m. The ballast water effects in the numerical simulation were converted into two additional stiffness values. Further details are given by (Robertson et al., 2014).

3.2. Validation load cases & results

Before running dynamic analysis, a static validation process, focusing on the horizontal restoring forces provided by the mooring lines, were carried out and compared with model tests data. Two validation processes were carried out. One has focuses on the static restoring performance, which is significant for setting up mooring line configurations for different water depths. The other focused on the free decay simulations and the natural frequencies in terms of supporting the platform's six degrees of freedom (DOFs).

3.2.1. Restoring forces

The load-offset graph in 200m water depth in the surge direction is shown in **Fig. 5**. The numerical tests were realised through setting different initial surge motions, ranging from zero to around 20 m. In **Fig. 5**, "Experiment" denotes the model test results from Dagher et al. (2017); Present (OrceFlex) and Present (FAST) indicated the numerical simulation results based on OrcaFlex ("Orcina Ltd,") and FAST (Jonkman and Jonkman, 2016), respectively. As can be seen, there is an excellent agreement between model test results and present results based on FAST, showing the validity of the present method in the forthcoming dynamic analysis regarding water depth effects. There is a minor difference for horizontal offsets larger than 10 m when compared to numerical simulation using OrcaFlex and model test results, but the overall agreement has reached a satisfying match, showing a good preparation for the subsequent case studies.

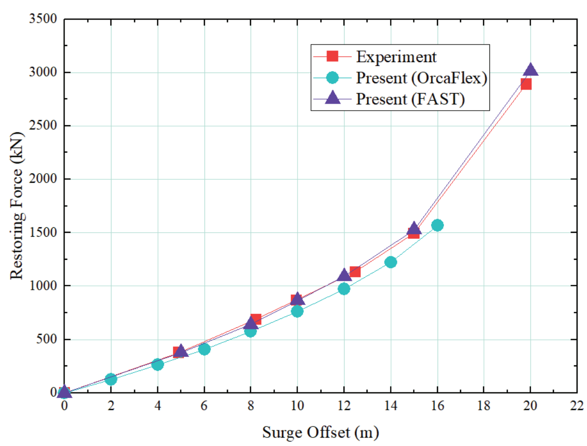

Figure 5 Static validation

3.2.2. Natural Frequencies

The second validation step has focused on the structure's natural frequencies. Six numerical free decay simulations were carried out based on each DOF's pre-subscribed initial positions. More specifically, for horizontal (surge and sway) motion DOFs, the initial offset was fixed at 10 m, while, for vertical DOF (heave), it had an initial offset of 3 m above the SWL. For rotational DOFs (roll, pitch and yaw), the initial angle was selected as 10 degrees. The free decay simulation was realised and carried out by disabling all the control capabilities and on a non-rotating turbine condition. To this end, the turbine generator DOF was also excluded during the simulation. All the free decay calculations were carried out in a no wind, wave or sea current condition. **Table 1** describes the comparison between the present numerical results and the model tests. All the comparisons have presented excellent agreements, except for the minor difference in roll and pitch DOFs. Nonetheless, the discrepancies are less than 3%, showing a great agreement between the present results and the model tests.

Table 1 Platform natural frequencies (present results and experimental results)

	Surge (Hz)	Sway (Hz)	Heave (Hz)	Roll (Hz)	Pitch (Hz)	Yaw (Hz)
Present	0.009	0.009	0.057	0.038	0.036	0.012
Experiment (Dagher et al., 2017)	0.009	0.009	0.057	0.037	0.037	0.012

4. Results & discussions

In this section, a list of load cases (LCs) for the analysis of water depth effects is described, followed by explanations of how the environmental conditions are calculated. All the LCs were simulated under a variety of water depths ranging from 200 to 300 m for both slack and taut mooring configurations. The total simulation time is one hour. Due to the application of a time-domain analysis, the initial 400s generate unstable results and this transient period was removed before carrying out post-processing investigations.

4.1. Load cases

As stated in section 1, it is valuable to investigate water depth effects under both healthy and failure conditions. Therefore, the proposed LCs are shown in **Table 2**. Two normal operating conditions are considered, where one LC's average wind speed locates in the below-rated wind range while the other LC has an average wind speed of the above-rated condition. Both wave heights and wave periods are selected in accordance with the average wind speed. For the failure LC, this paper has focused on a grid loss condition and the forthcoming outcome of HSS brake, which is an important event to investigate the safe operating of FOWTs. During LC3, all the three blades are feathered after the failure happened (Jiang et al., 2014), the considered sea states include an average wind speed of 22 m/s (above-rated) and the same wave conditions as LC2.

Table 2. Environmental conditions and turbine operating status in the case studies (sea stated conditions from Qu et al. (2020))

LC	Wind speed (m/s)	Sea states			Turbine status
		Wave height (m)	Wave Period (s)	Current speed (m/s)	
1	8	1.67	8	0.5	Normal Operating

2	22	6.2	12.5	0.5	Normal Operating
3	22	6.2	12.5	0.5	HSS Brake due to grid loss

In the numerical simulation, the turbulence wind profile was pre-generated by an open-source tool TurbSim(Jonkman, 2009). The wind speeds in space were calculated based on Kaimal spectrum, with a standard turbulence intensity of the recommendation from IEC type A. An example of the undisturbed wind speed time history in the horizontal X-direction under LC2 (see **Table 2**) is described in **Fig. 6** for a total duration of one hour.

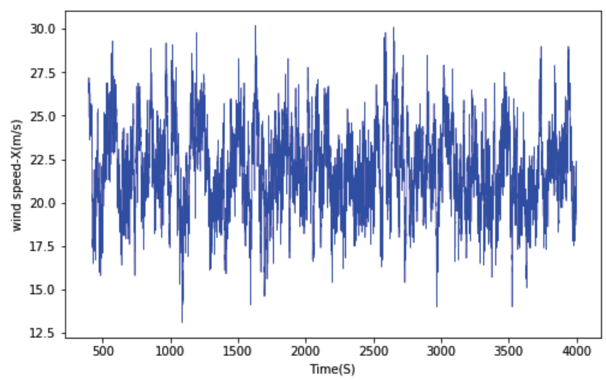

Figure 6 Horizontal undisturbed wind speed in the X direction (LC2 in Table 2)

The wave kinematics model was based on the Joint North Sea Wave Project (JONSWAP) spectrum with mono incident wave direction (Hasselmann et al., 1973):

$$S(\omega) = \frac{\alpha g^2}{\omega^5} exp\left[-\frac{5}{4}\left(\frac{\omega_P}{\omega}\right)^4\right]\gamma^r \quad (15)$$

$$r = exp\left[-\frac{(\omega-\omega_P)^2}{2\sigma^2\omega_p^2}\right] \quad (16)$$

where γ is the peak enhancement factor; γ=3.3.

Fig. 7 shows the incident wave spectrum for the first LC in **Table 2**. It has a significant wave height of 6.2 m and a peak period of 12.5s. The power spectrum was generated by the incident wave time series and normalised by the mean square value. The adjacent-averaging algorithm was applied to remove the noise of the spectrum with a moving window.

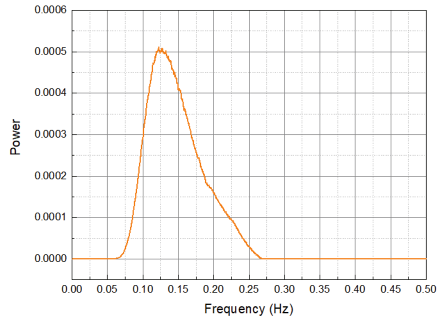

Figure 7 Incident wave spectrum (generated from wave elevation at platform centre of LC2)

4.2. Mooring configurations & load-offset relationships

Due to the large number of parameters related to water depth variations, it is necessary to limit the number of parameters, while at the same making responses results in different water depth more comparable. Based on the surge restoring force under different offsets for 200 m water depths in a slack mooring configuration (see **Fig. 5**), the principle of developing the mooring properties is to measure the surge load-offset relationship as accurate as possible (Ahmed Ali et al., 2019) (**Fig. 8**). **Table 3** shows the mooring positions (anchor) and line lengths for different water depths and configurations. The fairlead positions for different water depths remain the same as the original design of the OC4 semi-submersible type FOWT (Robertson et al., 2014) (200 m water depth, slack mooring configuration). Mooring line material for all the slack configurations utilized the same chain as in 200m water depth (Robertson et al., 2014). It has a mooring line length of 835.5m and an equivalent mooring line mass in water of 108.63 kg. The material for the taut mooring line is polyester. The nominal diameter for the polyester (0.2m) line is obtained from Azcon et al.(2017), and the remaining parameters based on the diameter is derived in OrcaFlex. More details of the properties for the two types of lines can be seen in **Table 4**.

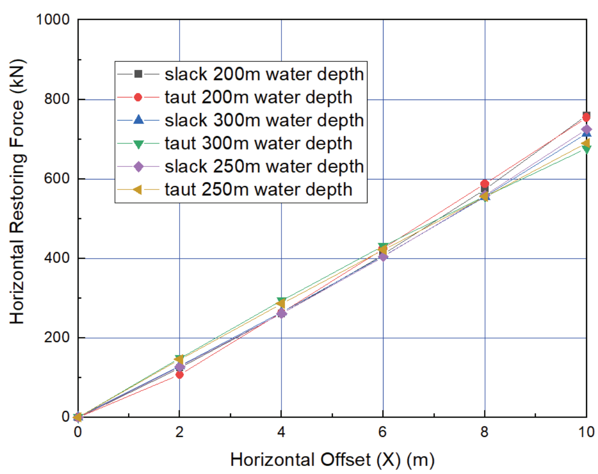

Figure 8. Horizontal (surge) offset for all the water depths

Table 3. Mooring line properties (Anchor)

Water depth (m)	Slack Mooring					Taut Mooring				
	length (m)	Line No.	X	Y	Z	length (m)	Line No.	X	Y	Z
200	835.5	1	418.8	725.4	-200.0	245.0	1	100.0	173.2	-200.0
		2	-837.6	0.0	-200.0		2	-200.0	0.0	-200.0
		3	418.8	-725.4	-200.0		3	100.0	-173.2	-200.0
250	1054.5	1	523.5	906.7	-250.0	314.5	1	125.0	216.5	-250.0
		2	-1047.0	0.0	-250.0		2	-250.0	0.0	-250.0
		3	523.5	-906.7	-250.0		3	125.0	-216.5	-250.0
300	1273	1	628.2	1088.0	-300.0	383.5	1	150.0	259.8	-300.0
		2	-1256.4	0.0	-300.0		2	-300.0	0.0	-300.0
		3	628.2	-1088.0	-300.0		3	150.0	-259.8	-300.0

Table 4 Parameters of slack and taut lines

Configuration	Material	Mass in water (kg/m)	EA (kN)
Slack	Studlink Chain	108.63	753600
Taut	Polyester	31.91	43600

4.3. Normal operating condition

4.3.1. Time-history results

- Statistics of motion responses

Compared with platform pitch responses, surge and heave motion responses are more affected by water depth (**Fig.9**). The static surge responses for different water depth and mooring configurations have been matched statically without environmental loadings (see **Fig.8**), resulting in the mean surge less dependent on the water depth. When considering a sever sea state (above-rated in **Fig.8**), water depth effects become important for the evaluation of maximum surge values, especially for taut lines. This is probably due to the different restoring forces levels provided between slack and taut lines. With the increasing of surge offset, the nonlinearity in the mooring stiffness is significant. Besides, the dynamic coupling effects could contribute to the discrepancy, as the matching Fig. 8 was carried out statically. The increased water depth has resulted in an apparent effect on the heave motion with slack mooring lines, while for taut lines the differences on heave motions between 200m and 300m water depths are almost ignorable (**Fig.9**). One reason for it is due to the different vertical components provided by slack and taut lines. For slack moorings, the steeper fairlead angle contributes to a higher vertical force component than the taut counterpart (Bach-Gansmo et al., 2020).

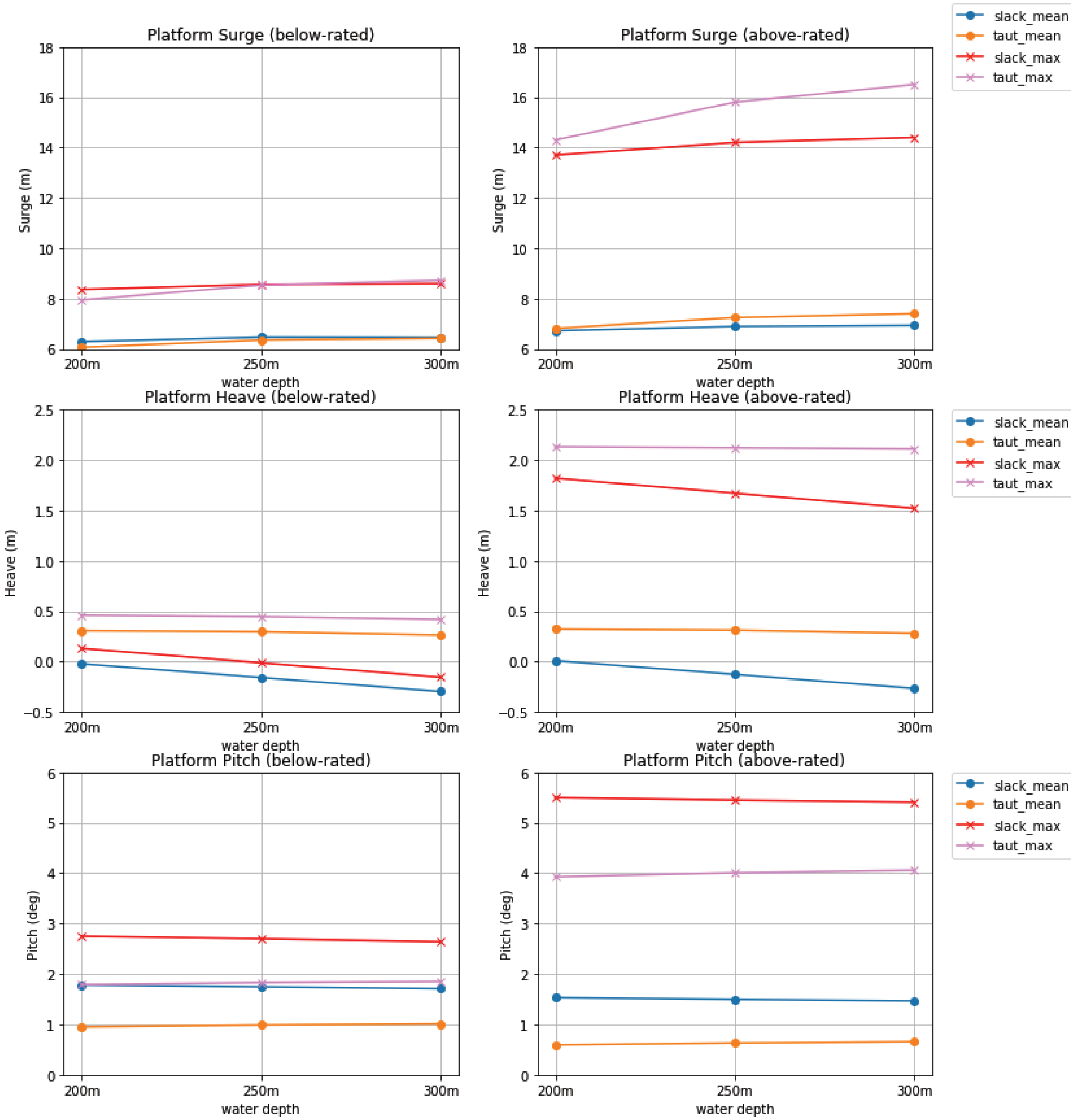

Figure 9 Statistical results of platform motions for slack & taut moorings (LC1: below-rated; LC2: above-rated)

- Spectra of motion responses

To further examine the reason for the discrepancies in statistical results, the power spectral density (PSD) of the motion time history is shown in **Fig. 10** and **Fig. 11**. The PSD was evaluated by Welch's average periodogram method (Welch, 1967). As can be seen from the figures, the spectra are all dominated by a frequency range of less than 0.2 Hz. All the major discrepancies are observed for the frequency range above 0.4 Hz (**Fig. 10** and **Fig. 11**). In addition, the variation of water depth has an influence on the low-frequency range of heave responses (below 0.1 Hz).

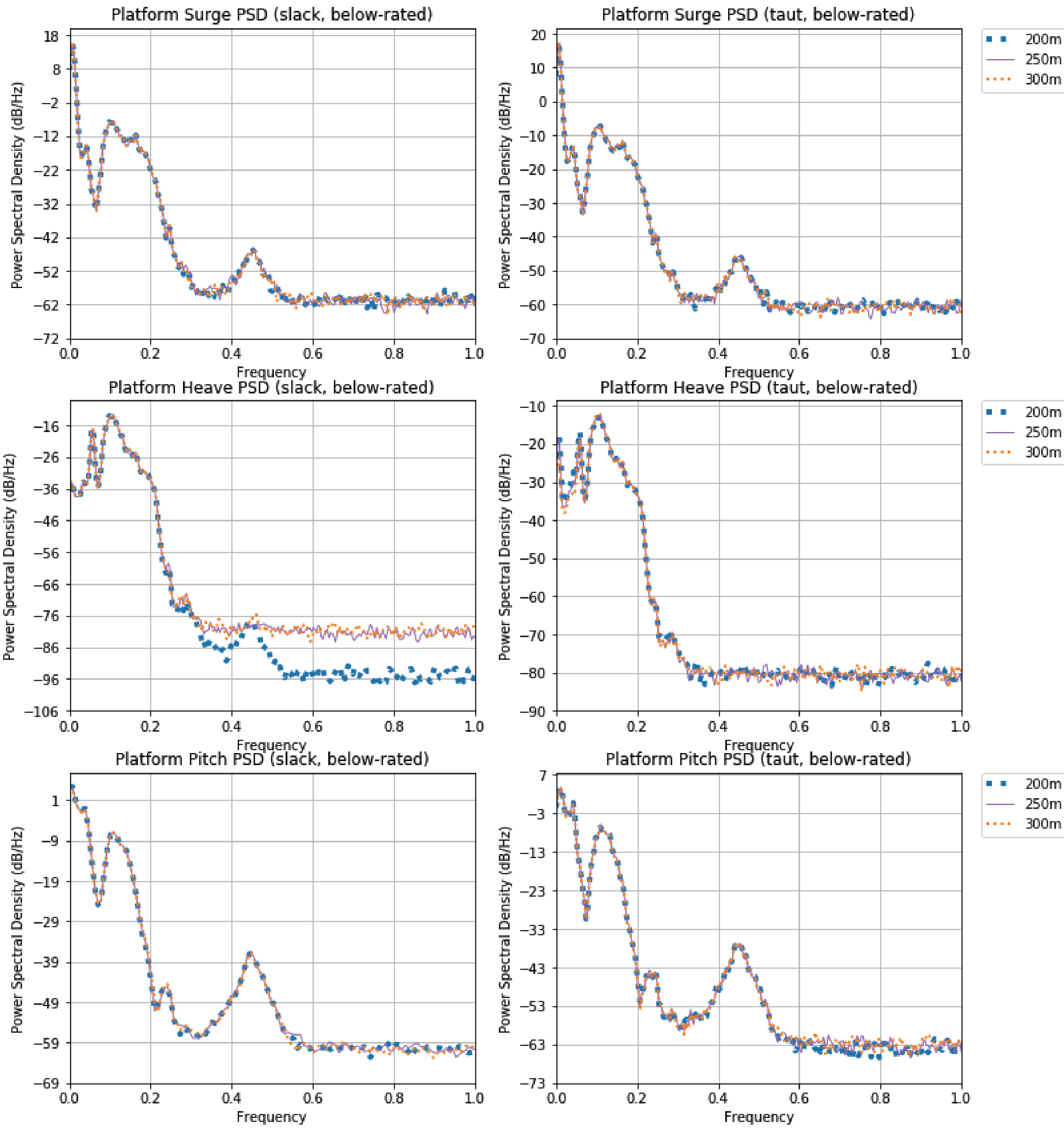

Figure 10 PSD of platform motions (LC1, slack & taut moorings)

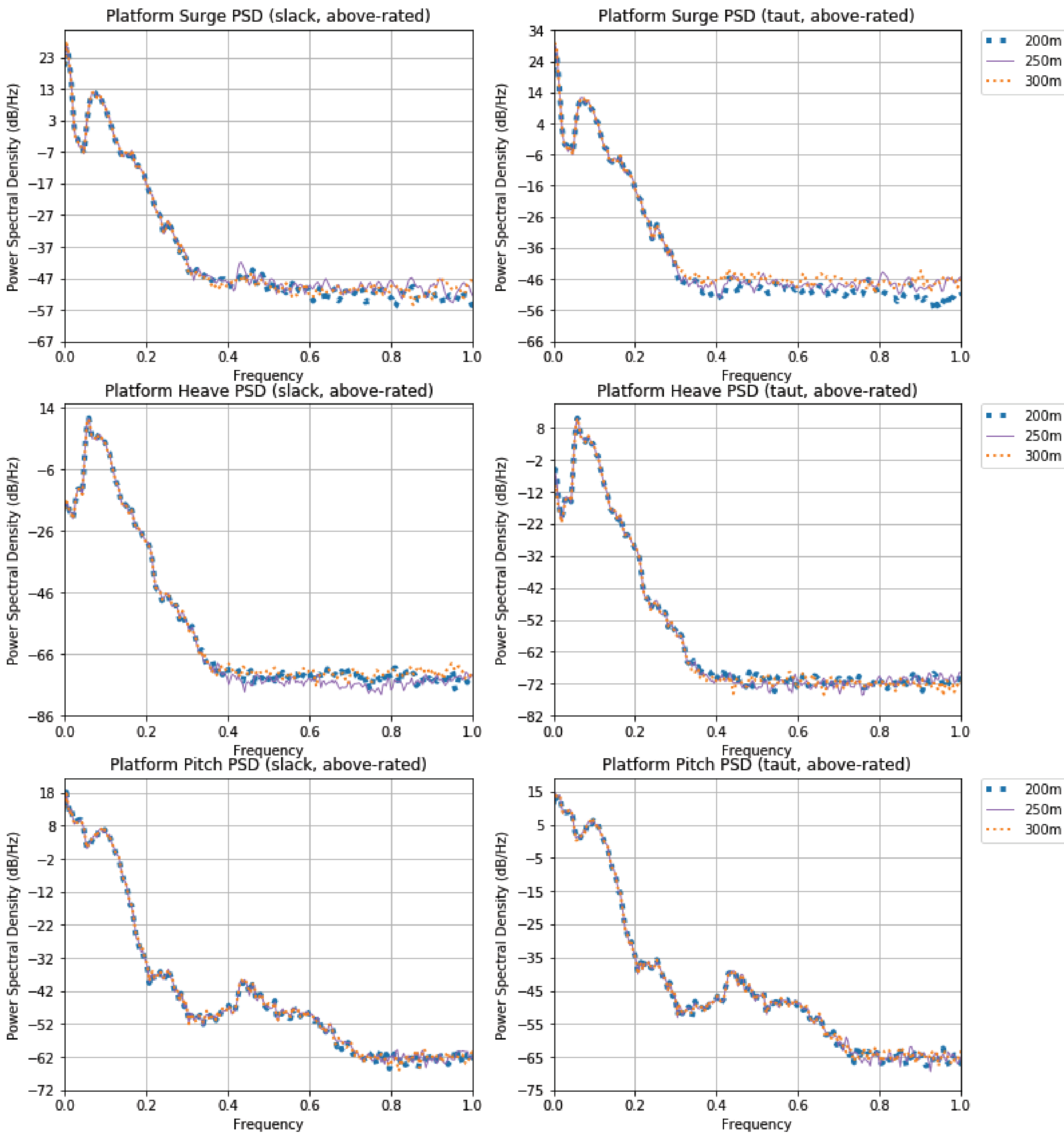

Figure 11 PSD of platform motions (LC2, slack & taut moorings)

- Mooring line tensions

For slack moorings, both mean and maximum values increase with the growth of water depths, while taut moorings are less sensitive to water depth variations (**Fig.12**). Slack mooring configuration tends to significantly enlarge its maximum mooring line tension with the increasing of water depths. This trend showed an agreement with the corresponding power spectra as shown in **Fig.13**. All the mooring line tension PSD are in consistence with platform surge motion, caused by the incident wave spectra, regardless of below or above wind conditions. These phenomena show that the mooring line top tension is mainly driven by the surge motion. With the increase of water depth, the discrepancies regarding PSD are more significant on the slack mooring configuration than the taut configuration (see **Fig. 13**). For slack moorings, this discrepancy is mainly centred at a frequency range of below 0.25 Hz. While for taut moorings, the differences are more significant for a frequency range below 0.1 Hz in above-rated condition (see **Fig. 13**).

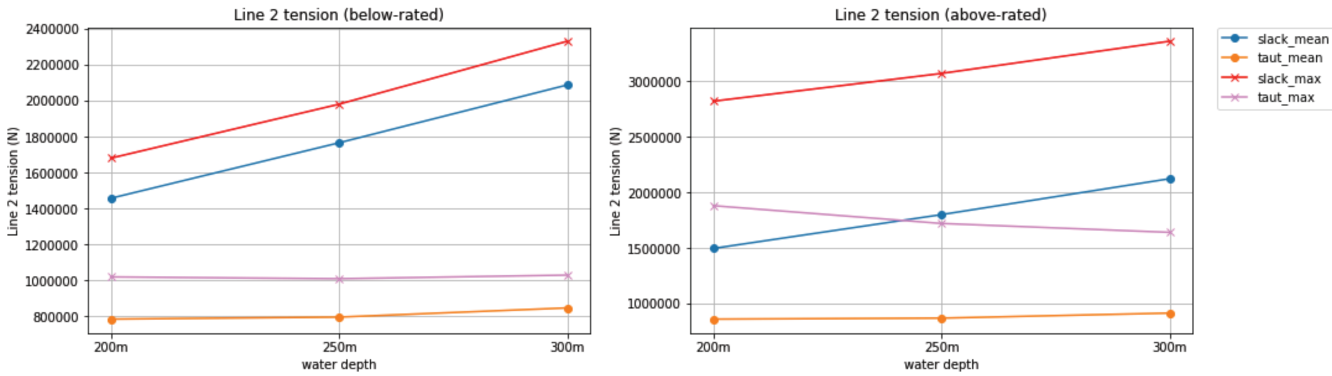

Figure 12 statistical results of line 2 top tension (LC1, LC2, slack & taut)

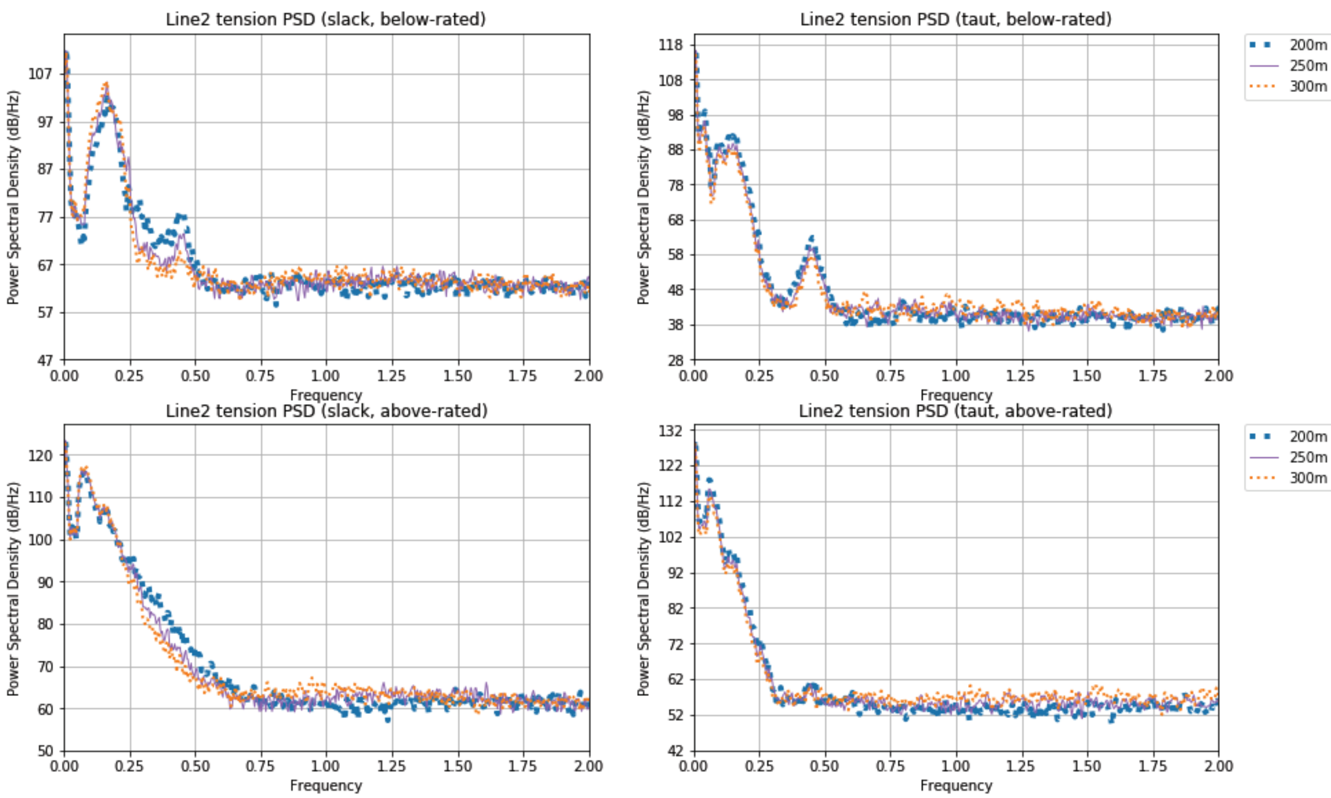

Figure 13 PSD of line 2 top tension (LC1, LC2, slack & taut)

On the contrary to the significant effects from platform motions and most loaded line (line 2) top tensions, wind turbine power output and tower base forces are almost independent of water depths (see **Fig. 14~15**). Compared with the fore-aft force

(TwrBsFxt), tower base side-side force (TwrBsFyt) performed differently with the increasing of water depth, but the discrepancies are less significant, which can be further proved from the PSD as shown in **Fig.15**.

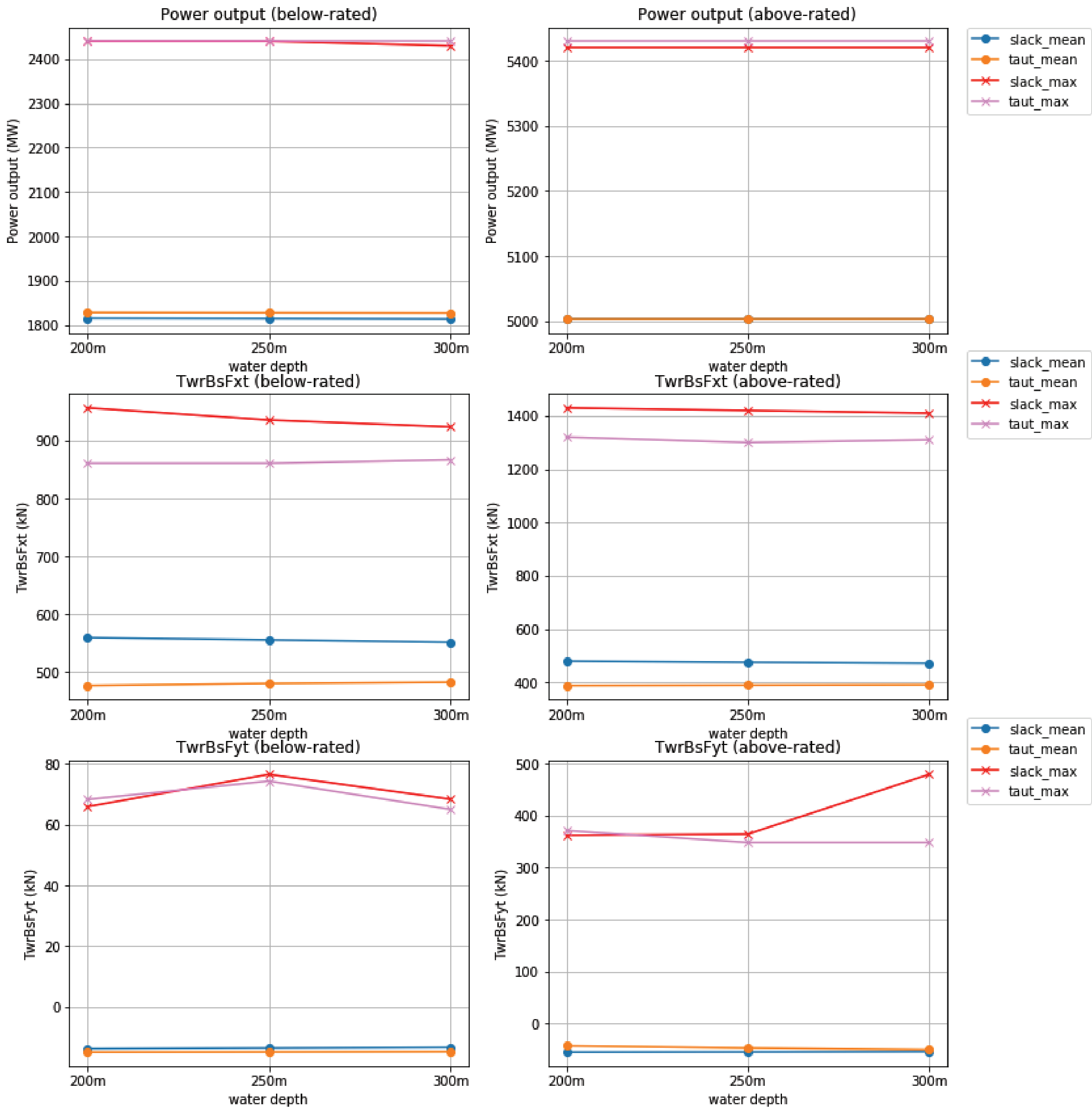

Figure 14 statistical results of wind turbine power output and tower base forces (LC1 &LC2, slack & taut moorings)

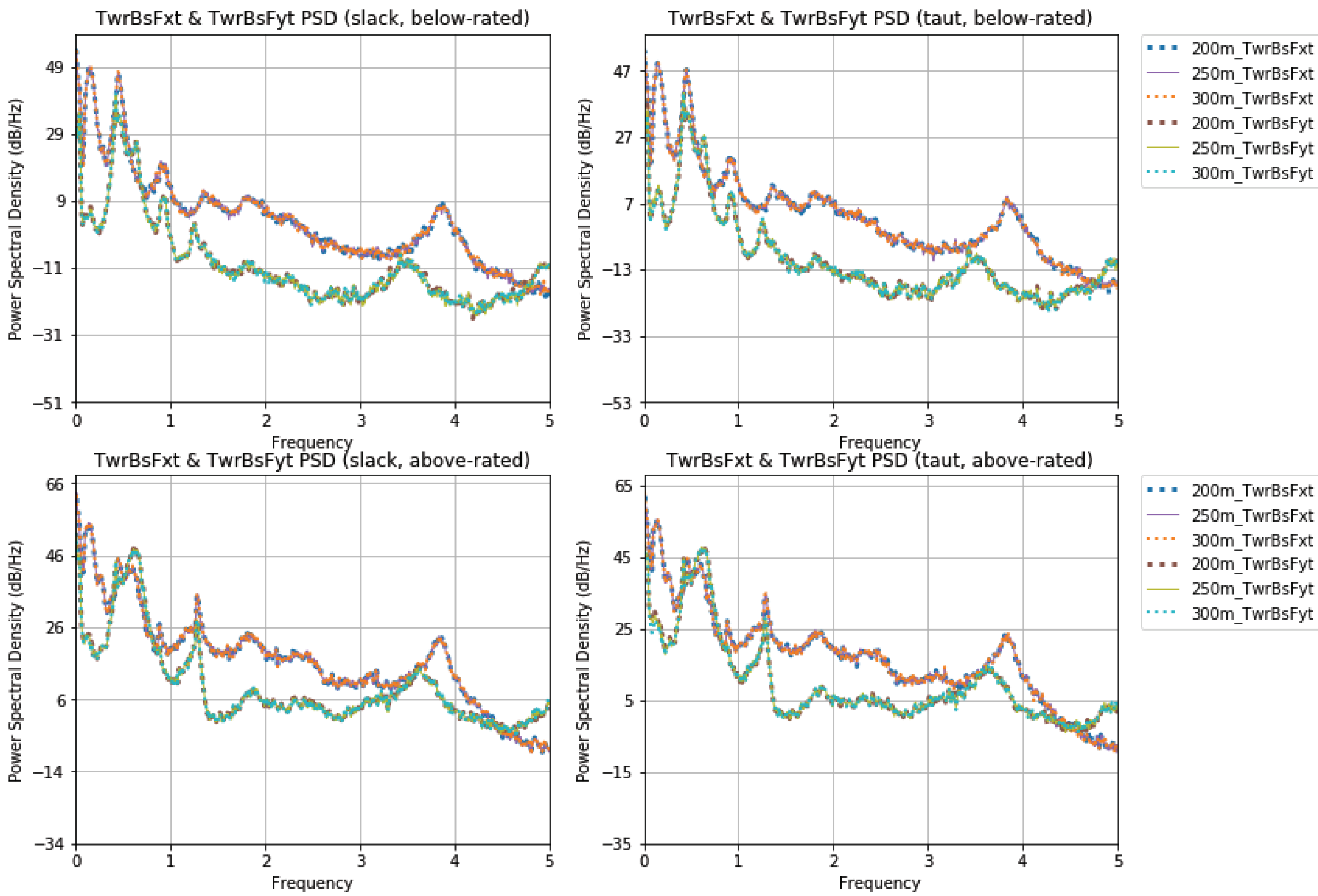

Figure 15 PSD of tower base bending forces (LC1 & LC2, slack & taut moorings)

4.3.2. Fatigue results

Section 4.3.1 has discussed the dynamic response characteristics in terms of statistical results and spectra. In this section, responses and performances of the FOWT under a variety of water depth are compared and discussed based on short-term DELs. The calculation methods for generating the DELs have been introduced in section 2.1.5, which include a computation using a fixed mean value and the Goodman correction. **Fig.16** and **Fig.17** show a description of calculated DELs under different environmental (below-rated and above-rated) and mooring conditions. As can be seen, compared with tower DELs, mooring line DELs performed differently with the increase of water depth. Comparing against different mooring configurations, taut moorings are expected to have larger DELs, which are almost double of that of slack mooring lines with catenary chains. As for the tower DELs, there are almost no significant differences under different environmental (below-rated and above-rated conditions) conditions and mooring configurations. There are only minor differences for tower base DEL (side-side bending force) under slack mooring configuration, showing a slight rise of DEL with the growth of water depth.

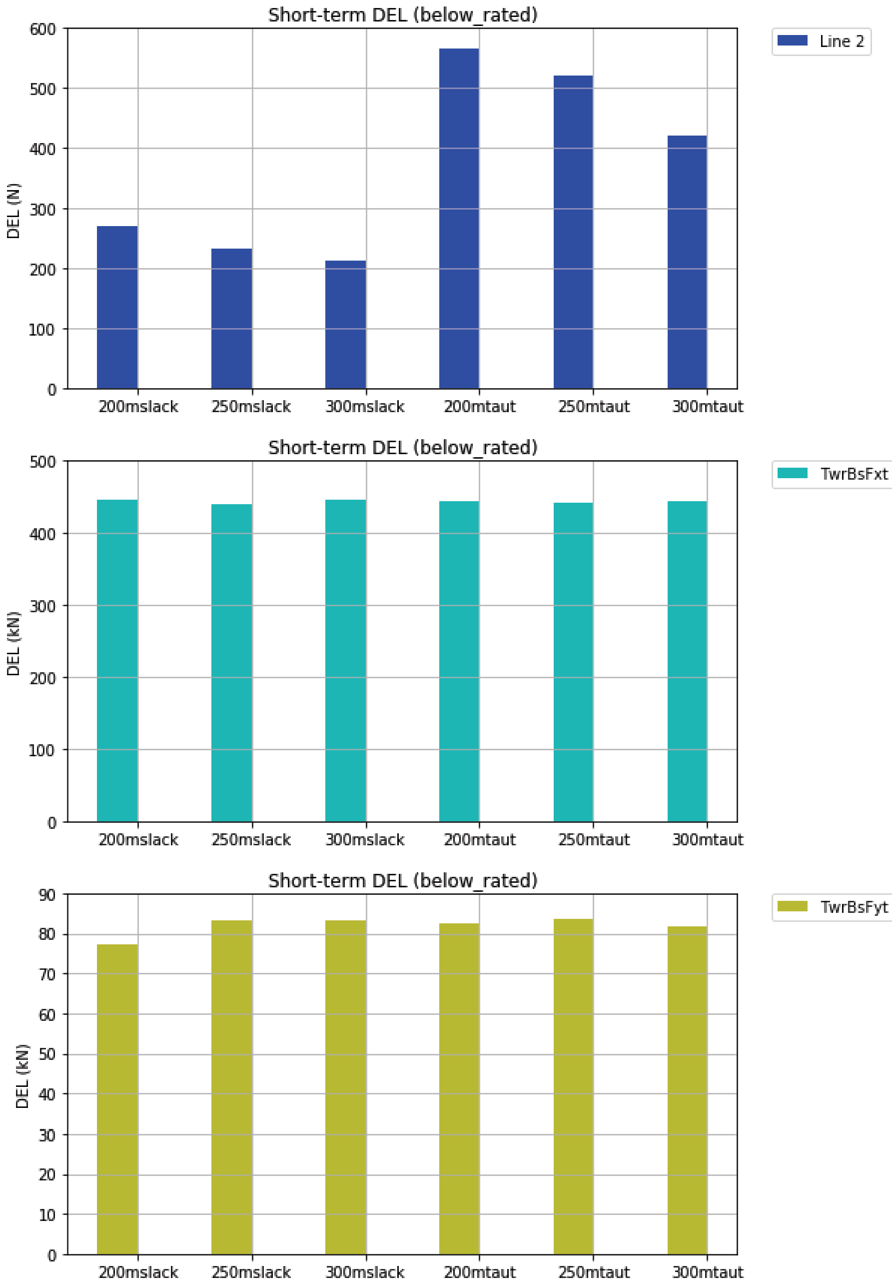

Figure 16 DEL of line 2 top tension and tower base forces (LC1)

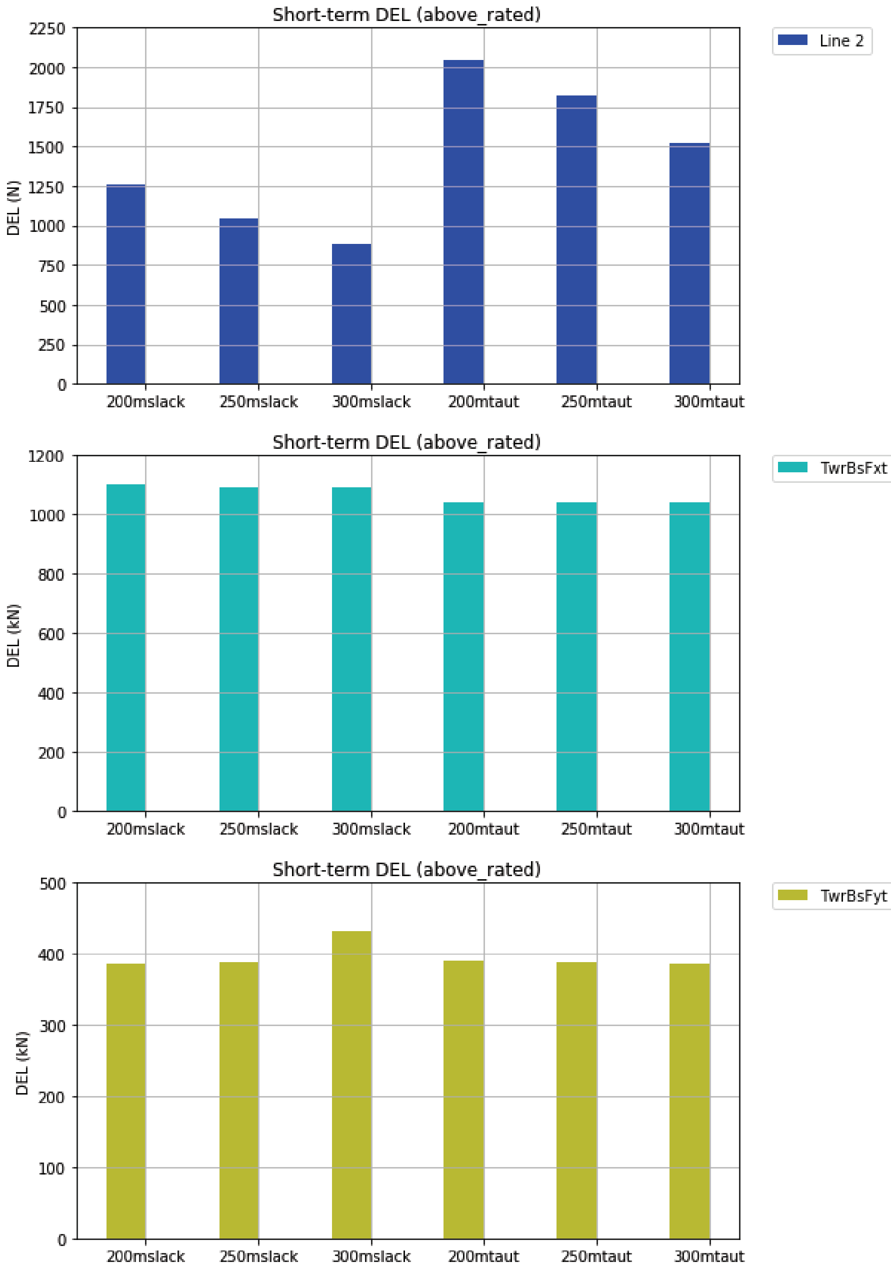

Figure 17 DEL of line 2 top tension and tower base forces (LC2)

4.4. Grid loss induced HSS break event

Section 4.3 has focused on analysing water depths effects under normal turbine operating conditions. For safe operation of the wind turbine, it is significant to explore the global responses with water depth increasing under a certain failure condition. In this section, the turbine special event with grid loss failure was carried out in a wind, wave and current sea environment. Only above-rated wind speeds are considered, as the three blades feathered after the failure event happened (Jiang et al., 2014). The shaft brake torque (28116.2 N·m) follows a linear ramp function from zero to full.

Transient behaviour of platform motions, mooring line tension and tower base forces are shown in **Fig. 18**, **Fig.19** and **20**, respectively. The grid loss event and the high-speed shaft (HSS) break started at the 1500 s, where the total simulation time is 1 hour. The grey background in **Fig. 18**, **Fig.19** and **20** describes the time history of the failure. As presented, the failure event has a greater influence on the transient surge motion responses and mooring line tensions (**Fig. 18** and **Fig.19**), but less affected the heave motion responses, regardless of mooring system configurations. The response spectra, which was described in **Fig. 21** and **Fig.22**, only considered the time series after a failure occurred. Compared with turbine healthy conditions, a similar trend has investigated on mooring line tension spectra, for which slack mooring line responses are more water-depth sensitive than the taut lines (**Fig.13** and **Fig.22**).

The failure event has a more obvious influence on the tower side-side bending force, compared with the fore-after bending force. As can be seen in **Fig. 23**, water depth increasing has contributed to the difference in tower base bending forces (above 2Hz). In addition, the maximum bending forces are no longer water-independent, especially for the fore-aft direction (see **Fig. 14** and **Fig.24**), but the overall discrepancies are still less significant compared with the mooring line top tension discrepancies.

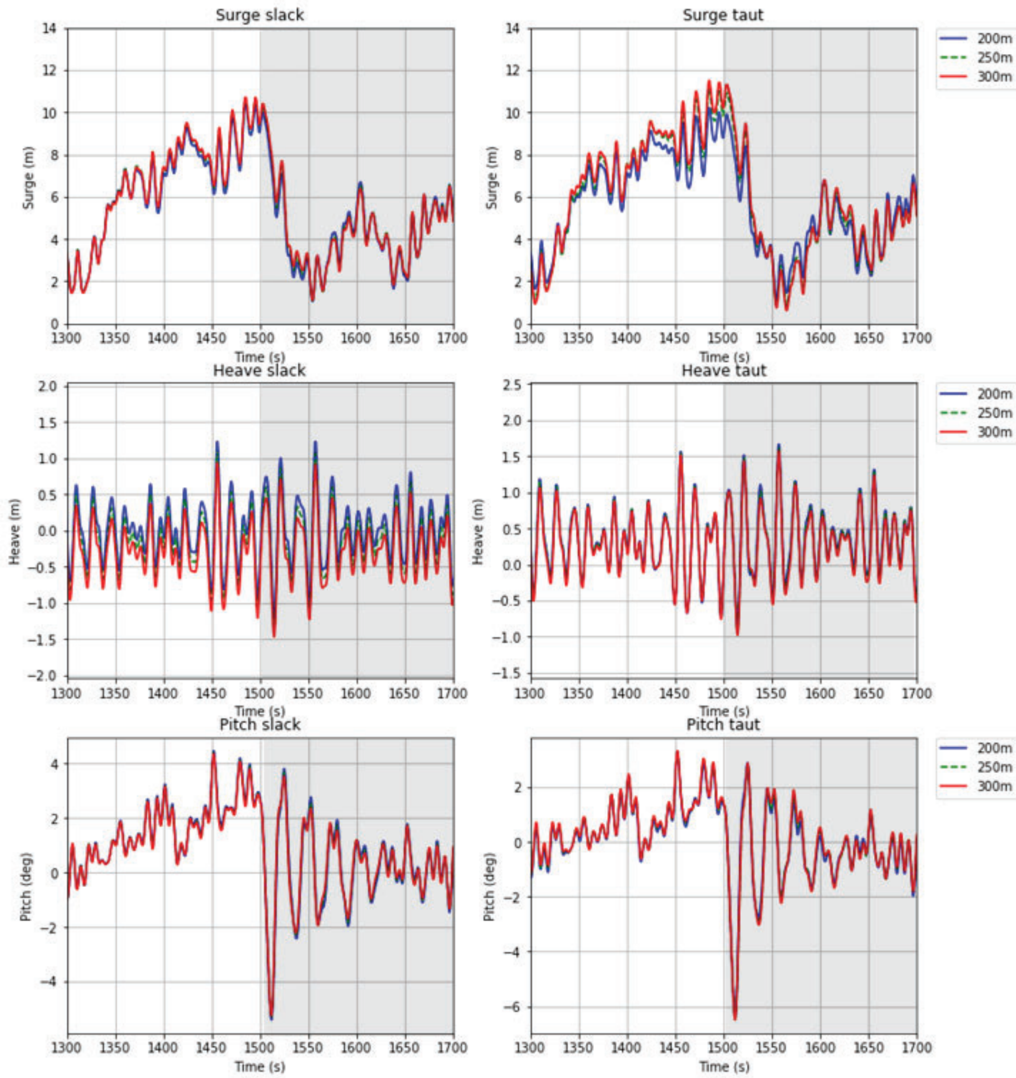

Figure 18 Transient behaviour of platform motions (LC3)

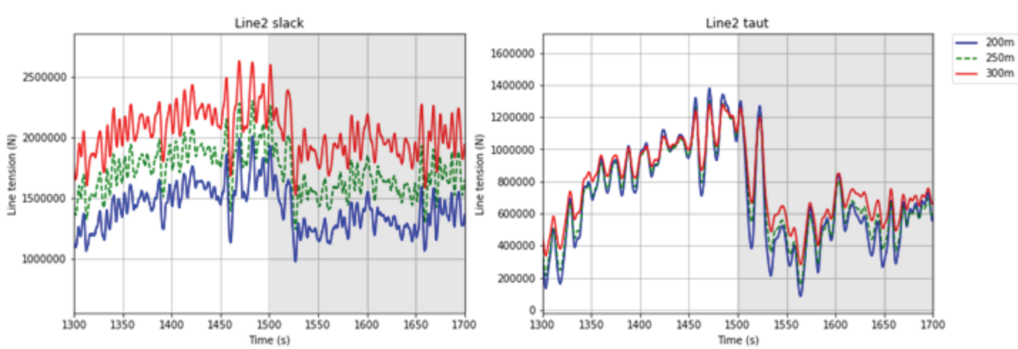

Figure 19 Transient behaviour of the most loaded line tension (LC3)

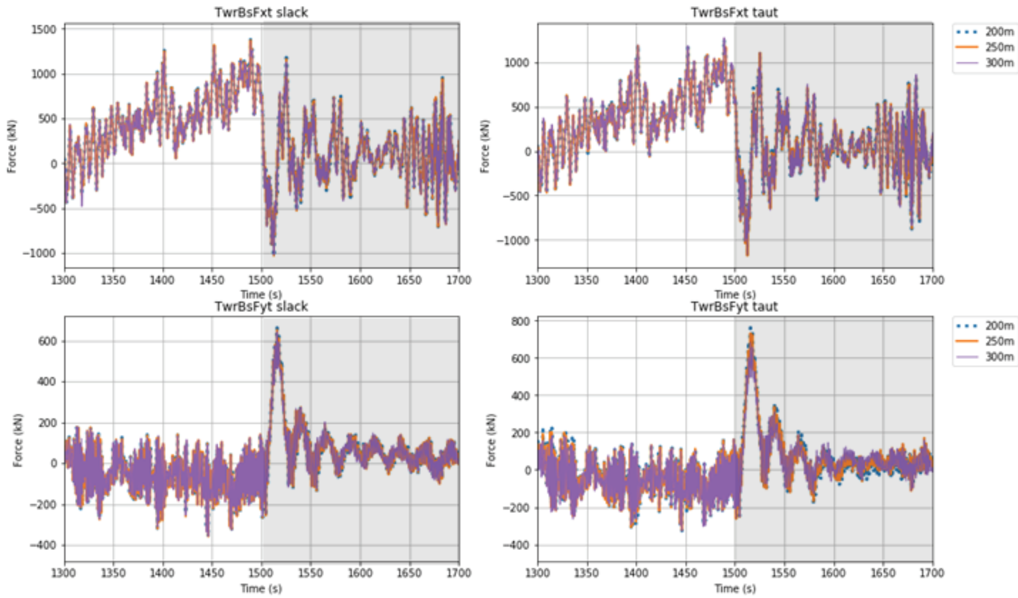

Figure 20 Transient behaviour of tower base forces (LC3)

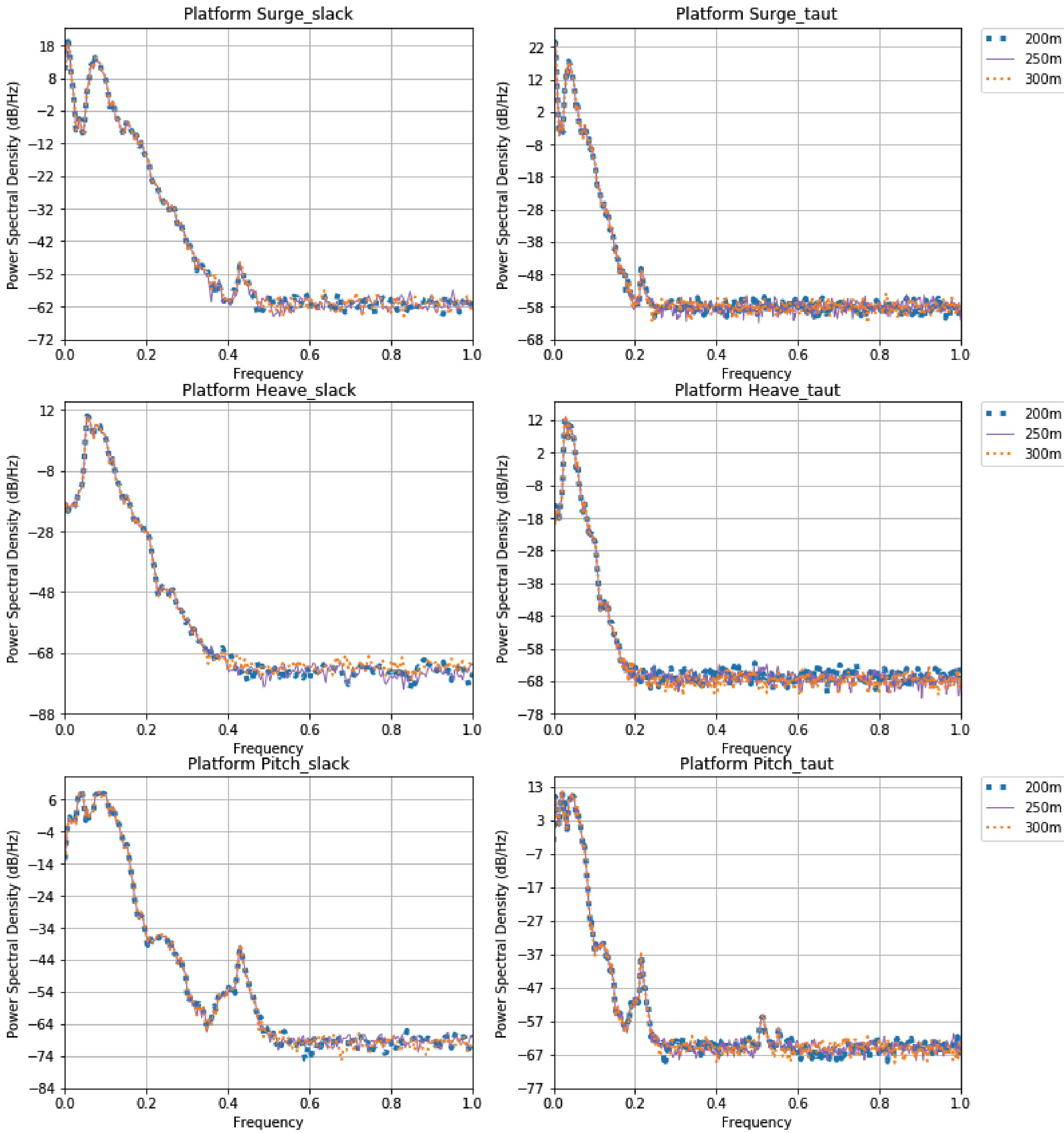

Figure 21 Spectra of platform motions (LC3)

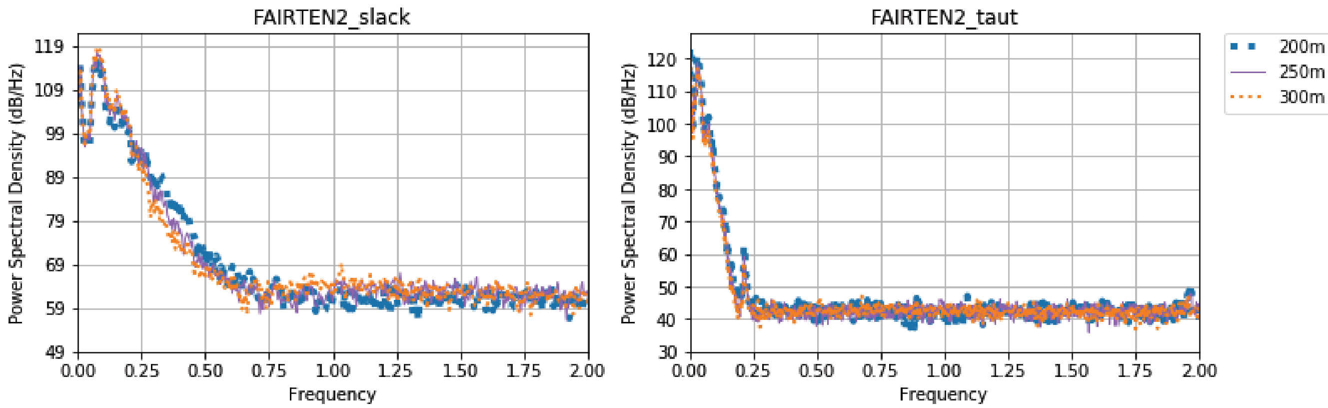

Figure 22 Spectra of mooring line tension (LC3)

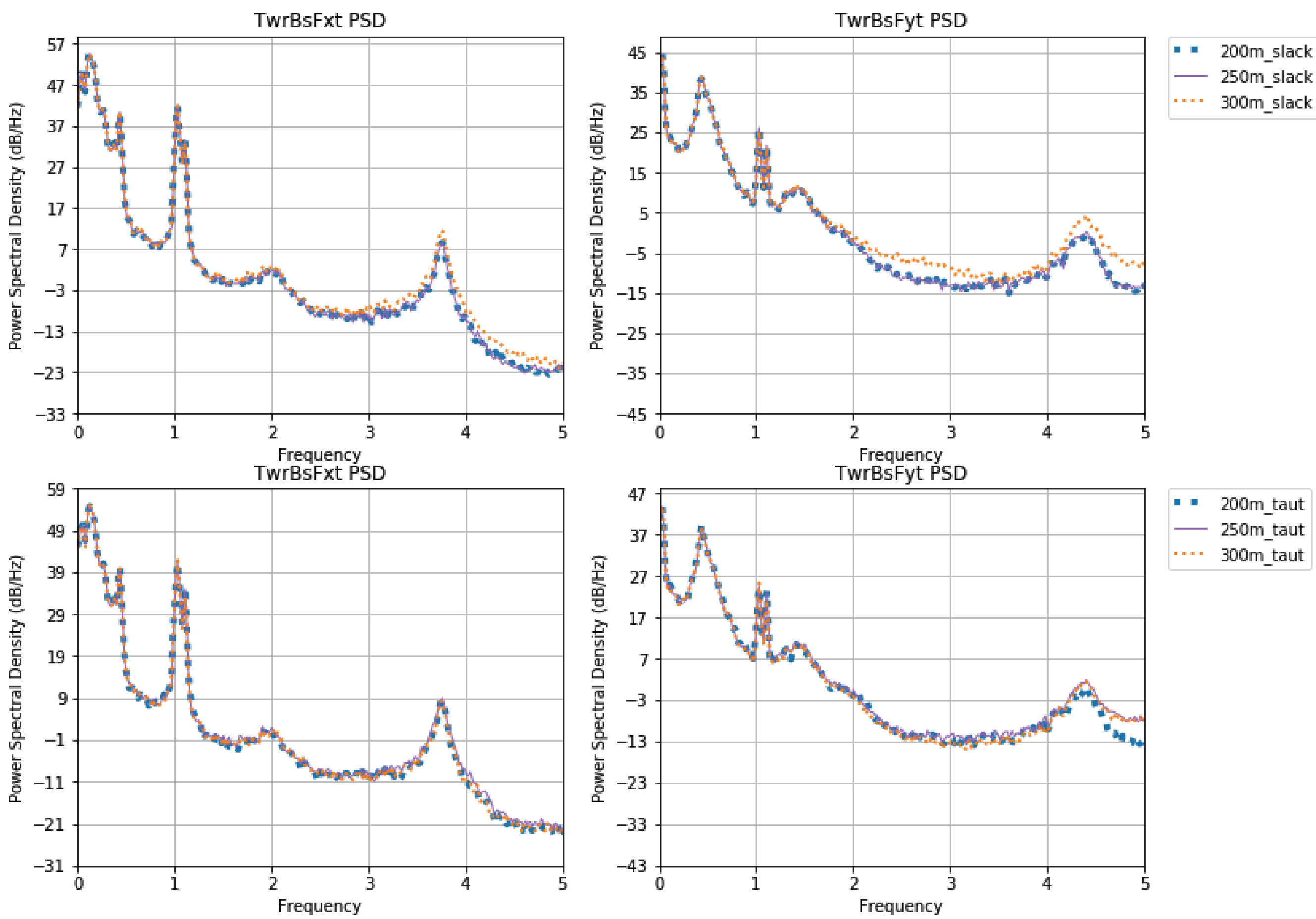

Figure 23 Spectra of tower base forces (LC3)

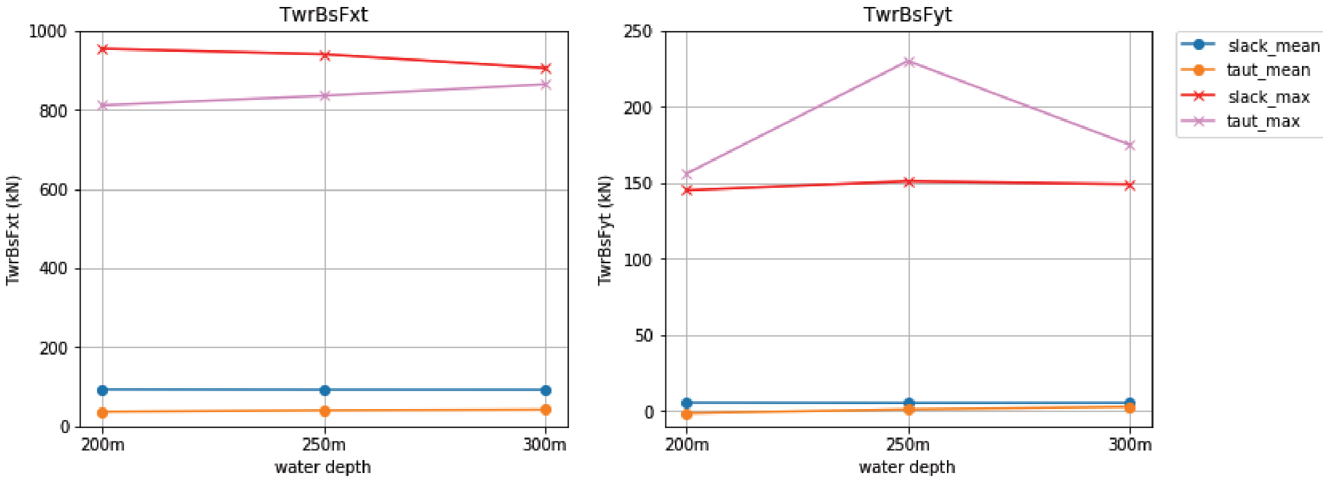

Figure 24 Statistical results of tower base forces (LC3)

5. Conclusions

This study critically analysed the effects of water depth increase on the global performance of FOWTs. The principle of comparison among various water depths lies in keeping the horizontal (surge) static restoring force measured as close as possible. Based on this principle, mooring system properties for both slack and taut configurations were derived based on the original design of the OC4 semi-submersible FOWT. The simulation results were validated against technical data in the public domain, where a great agreement was reached. Before carrying out time-series and fatigue analysis, a number of case studies were put forward in a combined wind, wave and current circumstance under considerations of different turbine operating conditions. Based on the case studies and the post-processing procedure, the following conclusions can be derived:

- For platform motion responses, heave motion with a catenary configuration tends to increase obviously with the growth of water depth, which is because of the steepness of slack moorings in the fairlead and the large vertical force components in larger water depth. For future wind turbines (e.g. 20MW) operated in much deeper water depth (e.g. more than 500 m), taut moorings are expected to outperform slack moorings in terms of vertical motions.
- Compared with surge and pitch motion responses, mooring line top tensions are more sensitive to water depth, regardless of environmental conditions. The increasing of water depth impact the DEL of both slack and taut mooring configurations, but taut moorings are of higher DELs than that of slack moorings.
- Tower base bending forces are almost water-depth independent under normal operating conditions, regardless of below or above wind speeds, but a grid loss event including HSS brake will trigger a discrepancy on the high-frequency (>2Hz) responses of tower base bending forces with an escalation of water depth.

Acknowledgement

The third author is supported by the UK Engineering and Physical Sciences Research Council (EPSRC) CAMREG project (Ref. No. EP/P007805/1).

References

Aggarwal, N., Manikandan, R., Saha, N., 2017. Nonlinear short term extreme response of spar type floating offshore wind turbines. Ocean Eng. 130, 199–209. https://doi.org/10.1016/j.oceaneng.2016.11.062

Ahmed Ali, M.O., Ja'e, I.A., Zhen Hwa, M.G., 2019. Effects of water depth, mooring line diameter and hydrodynamic coefficients on the behaviour of deepwater FPSOs. Ain Shams Eng. J. 11, 727–739. https://doi.org/10.1016/j.asej.2019.12.001

Azcon, J., Vittori, F., Savenije, F., Kapogiannis, G., Karvelas, X., Manolas, D., Voutsinas, S., Amann, F., Ricardo, F.-G., Lemmer, F., 2017. Design Solutions for 10MW Floating Offshore Wind Turbines.

Bach-Gansmo, M.T., Garvik, S.K., Thomsen, J.B., Andersen, M.T., 2020. Parametric study of a taut compliant mooring system for a FOWT compared to a catenary mooring. J. Mar. Sci. Eng. 8. https://doi.org/10.3390/JMSE8060431

Bae, Y.H., Kim, M.H., Kim, H.C., 2017. Performance changes of a floating offshore wind turbine with broken mooring line. Renew. Energy 101, 364–375. https://doi.org/10.1016/j.renene.2016.08.044

Bayati, I., Gueydon, S., Belloli, M., 2015. Study of the Effect of Water Depth on Potential Flow Solution of the OC4 Semisubmersible Floating Offshore Wind Turbine. Energy Procedia 80, 168–176. https://doi.org/https://doi.org/10.1016/j.egypro.2015.11.419

Bir, G.S., 2007. User's guide to BModes. Natl. Renew. Energy Lab.

Chen, X., Yu, H., Wang, W., Wang, B., 2019. Analysis of Motion Response of Wind Turbine Platform Considering Different Heading Angles and Water Depths, in: 2019 2nd International Conference on Sustainable Energy, Environment and Information Engineering (SEEIE 2019). Atlantis Press, pp. 236–242. https://doi.org/https://doi.org/10.2991/seeie-19.2019.55

Cummins, W.E., 1962. The impulse response function and ship motions, in: Symposium on Ship Theory. Institut flir Schiffbau der Universitit Hamburg.

Dagher, H., Viselli, A., Goupee, A., Allen, C., 2017. 1:50 Scale Testing of Three Floating Wind Turbines at MARIN and Numerical Model Validation Against Test Data.

Deo, R.C., Ghorbani, M.A., Samadianfard, S., Maraseni, T., Bilgili, M., Biazar, M., 2018. Multi-layer perceptron hybrid model integrated with the firefly optimizer algorithm for windspeed prediction of target site using a limited set of neighboring reference station data. Renew. Energy 116, 309–323. https://doi.org/https://doi.org/10.1016/j.renene.2017.09.078

Duarte, T.M., Sarmento, A.J., Jonkman, J., 2014. Effects of second-order hydrodynamic forces on floating offshore wind turbines, in: 32nd ASME Wind Energy Symposium. American Institute of Aeronautics and Astronautics Inc. https://doi.org/10.2514/6.2014-0361

Durakovic, A., 2020. UK Prime Minister: Offshore Wind to Power Every Home by 2030 [WWW Document]. URL https://www.offshorewind.biz/2020/10/06/uk-prime-minister-offshore-wind-to-power-every-home-by-2030/

Goupee, A.J., Koo, B.J., Kimball, R.W., Lambrakos, K.F., Dagher, H.J., 2014. Experimental Comparison of Three Floating Wind Turbine Concepts. J. Offshore Mech. Arct. Eng. 136. https://doi.org/10.1115/1.4025804

Hall, M., 2017. MoorDyn User ' s Guide. Manual.

Hall, M., Goupee, A., 2015. Validation of a lumped-mass mooring line model with DeepCwind semisubmersible model test data. Ocean Eng. 104, 590–603. https://doi.org/10.1016/j.oceaneng.2015.05.035

Hasselmann, K., Barnett, T.P., Bouws, E., Carlson, H., Cartwright, D.E., Enke, K., Ewing, J.A., Gienapp, H., Hasselmann, D.E., Kruseman, P., Meerburg, A., Müller, P., Olbers, D.J., Richter, K., Sell, W., Walden, H.,

1973. Measurements of wind-wave growth and swell decay during the Joint North Sea Wave Project (JONSWAP).

Hayman, G., 2012. Mlife [WWW Document]. URL https://www.nrel.gov/wind/nwtc/mlife.html (accessed 9.17.20).

IEC, 2019. Wind energy generation systems - Part 3-1: Design requirements for fixed offshore wind turbines.

Jiang, Z., Karimirad, M., Moan, T., 2014. Dynamic response analysis of wind turbines under blade pitch system fault, grid loss, and shutdown events. Wind Energy 17, 1385–1409. https://doi.org/10.1002/we.1639

Jonkman, B.J., 2009. TurbSim User's Guide: Version 1.50. Golden.

Jonkman, B.J., Jonkman, J.M., 2016. FAST v8.16.00a-bjj User's Guide. Golden.

Journée, J.M.J., Massie, W.W., 2001. Offshore Hydromechanics. Delft University of Technology.

Le, C., Yane, L., Ding, H., 2019. Study on the Coupled Dynamic Responses of a Submerged FloatingWind Turbine under Different Mooring Conditions. Energies 12. https://doi.org/10.3390/en12030418

Luo, Y., Baudic, S., 2003. Predicting FPSO responses using model tests and numerical analysis. Proc. Int. Offshore Polar Eng. Conf. 5, 167–174.

Miner, M.A., 1945. Cumulative Damage in Fatigue. J. Appl. Mech. 3, 159–164.

Moriarty, P.J., Hansen, A.C., 2005. AeroDyn Theory Manual. Golden. https://doi.org/10.1146/annurev.fl.15.010183.001255

Morison, J.R., Johnson, J.W., Schaaf, S.A., 1950. The Force Exerted by Surface Waves on Piles. J. Pet. Technol. 2. https://doi.org/10.2118/950149-G

Nagababu, G., Kachhwaha, S.S., Savsani, V., 2017. Estimation of technical and economic potential of offshore wind along the coast of India. Energy 138, 79–91. https://doi.org/https://doi.org/10.1016/j.energy.2017.07.032

Newman, J.N., 1974. Second-order, Slowly-varying Forces on Vessels in Irregular Waves, in: Proceedings of International Symposium on Dynamics of Marine Vehicles and Structures in Waves. London.

OrcaFlex [WWW Document], n.d. . Orcina Ltd. URL https://www.orcina.com/orcaflex/

Ozturk, S., Fthenakis, V., Faulstich, S., 2018. Failure modes, effects and criticality analysis for wind turbines considering climatic regions and comparing geared and direct drive wind turbines. Energies 11. https://doi.org/10.3390/en11092317

Qu, X., Li, Y., Tang, Y., Chai, W., Gao, Z., 2020. Comparative study of short-term extreme responses and fatigue damages of a floating wind turbine using two different blade models. Appl. Ocean Res. 97, 102088. https://doi.org/10.1016/j.apor.2020.102088

Roald, L., Jonkman, J., Robertson, A., Chokani, N., 2013. The Effect of Second-order Hydrodynamics on Floating Offshore Wind Turbines. Energy Procedia 35, 253–264. https://doi.org/https://doi.org/10.1016/j.egypro.2013.07.178

Robertson, A., Jonkman, J., Masciola, M., Song, H., 2014. Definition of the Semisubmersible Floating System for Phase II of OC4.

Simos, A.N., Ruggeri, F., Watai, R.A., Souto-Iglesias, A., Lopez-Pavon, C., 2018. Slow-drift of a floating wind turbine: An assessment of frequency-domain methods based on model tests. Renew. Energy 116, 133–154. https://doi.org/https://doi.org/10.1016/j.renene.2017.09.059

Walsh, C., 2020. Offshore wind in Europe - Key trends and statistics 2019, Wind Europe. https://doi.org/10.1016/s1471-0846(02)80021-x

WAMIT® WAMIT, Inc. [WWW Document], n.d. URL http://www.wamit.com/

Welch, P.D., 1967. The Use of Fast Fourier Transform for the Estimation of Power Spectra: A Method Based on Time Averaging Over Short, Modified Periodograms. IEEE Trans. Audio Electroacoust. 15, 70–73. https://doi.org/10.1109/TAU.1967.1161901

Wen, T.R., Wang, K., Cheng, Z., Ong, M.C., 2018. Spar-Type Vertical-Axis Wind Turbines in Moderate Water Depth: A Feasibility Study. Energies 11, 1–17.